Three-dimensional convection in an inclined layer heated from below

F.H. BUSSE[1] and R.M. CLEVER[2]

[1]*Institute of Physics, University of Bayreuth, Universitätsstrasse 30, D-8580 Bayreuth, Germany*
[2]*Institute of Geophysics and Planetary Physics, University of California at Los Angeles, Los Angeles, CA 90024, USA*

Abstract. Longitudinal rolls aligned with the component of gravity parallel to the layer represent the preferred mode of convection at onset for a wide range of parameters of the inclined layer problem. As the Rayleigh number is increased beyond the critical value the longitudinal rolls tend to become unstable with respect to the wavy instability. The three-dimensional convection flows evolving from this instability are studied in this paper by numerical computations. The main effect of the wavy distortions of the longitudinal rolls is a decrease of the heat transport. The stability of the steady three-dimensional convection flow with respect to disturbances with the same periodicity interval in the plane of the layer is also investigated. Various instabilities are found in dependence on the Prandtl number P and the angle γ of inclination and their evolution is studied in a few cases.

1. Introduction

Convection in an inclined layer heated from below has been studied both experimentally and theoretically by numerous investigators during the past decades. In contrast to the case of a horizontal layer, the basic state of an inclined layer is characterized by a mean flow with a cubic profile. In the following we shall assume that the inclined layer is sufficiently extended that end effects do not affect the properties of convection flows very much. In particular we shall assume that the temperature distribution of the basic state is governed by conduction only and is approximately uniform throughout the plane of the layer.

The basic state of the inclined layer becomes unstable with respect to transverse or longitudinal rolls depending on the Prandtl number P of the fluid and on the angle of inclination. As discussed by Gershuni and Zhukhovitskii (1976) longitudinal rolls represent the preferred form of convection in high Prandtl number fluids for almost all inclinations as long as there exists a finite component of the temperature gradient opposite to the direction of gravity. Even in the case $P = 1$ longitudinal rolls remain preferred in an inclined layer heated from below up to an angle of 77° of inclination with respect to the horizontal. Only at much lower Prandtl numbers does the source of kinetic energy of the cubic profile flow contribute sufficiently to favor the onset of transverse rolls for all angles of inclination.

Longitudinal rolls are characterized by the property that their heat transport is independent of the angle γ of inclination if the normal component of gravity, $g \cos \gamma$, is used in the definition of the Rayleigh number. Other properties, however, such as the profile of the mean flow depend on the parameter γ. Accordingly, the stability properties of the longitudinal convection rolls also exhibit a strong dependence on the angle of inclination. In particular the wavy instability has been found to play a dominant role in restricting the region of the parameter space for which longitudinal rolls can be realized. For theoretical and experimental work on this topic we refer to the papers of Clever and Busse (1977, referred to in the following by CB77) and Ruth et al. (1980a). In the present paper we

investigate finite amplitude properties of three-dimensional wavy rolls induced by the onset of the wavy instability.

Convection in an inclined layer heated from below is of considerable interest for engineering applications. In particular, in the design of solar energy collectors the efficiency of the convective heat transport plays an important role. The fact that this efficiency is reduced significantly after the onset of wavy convection rolls has already been noted in the experimental study of Ruth et al. (1980a). The numerical results of the present paper provide details on the parameter dependence of this effect. Another effect emerging from the theoretical study of this paper is the onset of subcritical finite amplitude wavy rolls in some cases. This property may be responsible in part for some of the remaining discrepancies between experimental observations and the prediction of linear theory.

The mathematical formulation of the problem and the numerical method of solution are described in Section 2. While the basic equations are the same as those treated in CB77, three-dimensional solutions and their stability properties are analyzed in the present paper in contrast to the study of two-dimensional solution and their stability in CB77. The properties of steady wavy rolls are shown in Section 3 in comparison with those of longitudinal rolls. The results of the stability analysis together with the calculations for two time-dependent solutions are presented in Section 4 and a concluding discussion is given in the final section.

2. Mathematical description of the problem

We consider a fluid layer between parallel no-slip boundaries inclined at an angle γ with respect to the horizontal. Constant temperatures T_1 and $T_2(T_2 > T_1)$ are prescribed at the upper and lower boundaries. Using the thickness of the layer as length scale, d^2/κ as time scale where κ is the thermal diffusivity, and $(T_2 - T_1)/R$ as scale of the temperature we obtain the dimensionless form of the basic equations for a Boussinesq fluid as given by (2.1) of CB 77.

The basic state of the inclined layer as sketched in Fig. 1 is given by the dimensionless temperature distribution Θ_0 and the velocity field $\mathbf{U}_0$,
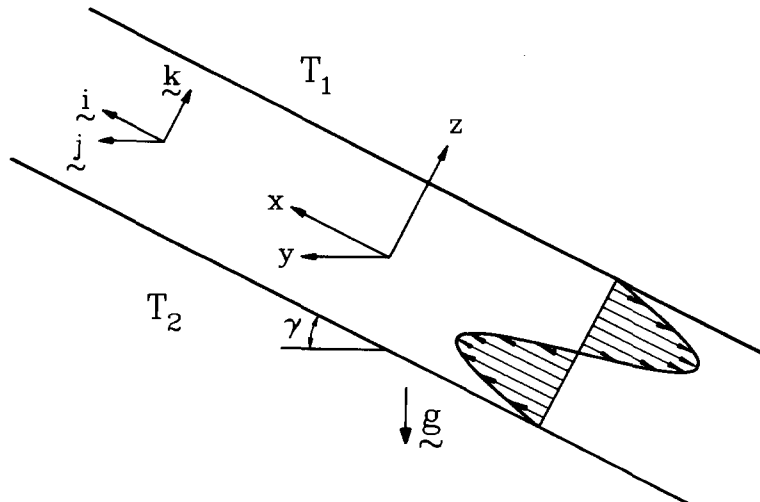

Fig. 1. Sketch of the geometrical configuration of the inclined layer heated from below.

$$\Theta_0 = -Rz + R(T_1 + T_2)/2(T_2 - T_1) , \qquad \mathbf{U}_0 = \mathbf{i}R\tfrac{1}{6}(z^3 - \tfrac{1}{4}z)\tan\gamma \equiv U_0\mathbf{i} , \qquad (2.1\mathrm{a,b})$$

where the Rayleigh number R is defined by

$$R = \beta g \cos\gamma (T_2 - T_1)\,\mathrm{d}^3/\nu\kappa . \qquad (2.2)$$

The coefficient β of thermal expansion, the acceleration g of gravity and the kinematic viscosity ν have been used in this expression. For the orientation of the coordinate system and the associated unit vectors $\mathbf{i}$, $\mathbf{j}$, $\mathbf{k}$ we refer to Fig. 1.

The secondary and tertiary solutions of the basic equations will be described as deviations from the primary solution (2.1),

$$\Theta = \Theta_0 + \vartheta , \qquad \mathbf{u} = U_0\mathbf{i} + U^{(x)}\mathbf{i} + \nabla\times(\nabla\times\mathbf{k}\varphi) + \nabla\times\mathbf{k}\psi \equiv U\mathbf{i} + \boldsymbol{\delta}\varphi + \boldsymbol{\varepsilon}\psi , \qquad (2.3\mathrm{ab})$$

where we have assumed that the x, y-average of the velocity field is directed solely in the x-direction.

By operating with $\mathbf{k}\cdot\nabla\times[\nabla\times\cdots]$ and $\mathbf{k}\cdot\nabla\times$ onto the equations of motion and using the heat equation we obtain the following three equations for φ, ω and ϑ,

$$\nabla^4\Delta_2\varphi + \tan\gamma\,\partial^2_{xz}\vartheta - \Delta_2\vartheta = P^{-1}\{\boldsymbol{\delta}\cdot[(\boldsymbol{\delta}\varphi + \boldsymbol{\varepsilon}\psi)\cdot\nabla(\boldsymbol{\delta}\varphi + \boldsymbol{\varepsilon}\psi)]$$
$$+ (U\partial_x + \partial_t)\nabla^2\Delta_2\varphi - \partial^2_{zz}U\partial_x\Delta_2\varphi\} , \qquad (2.4\mathrm{a})$$

$$\nabla^2\Delta_2\psi + \tan\gamma\,\partial_y\vartheta = P^{-1}\{\boldsymbol{\varepsilon}\cdot[(\boldsymbol{\delta}\varphi + \boldsymbol{\varepsilon}\psi)\cdot\nabla(\boldsymbol{\delta}\varphi + \boldsymbol{\varepsilon}\psi)] + (U\partial_x + \partial_t)\Delta_2\psi - \partial_z U\partial_y\Delta_2\varphi\} , \qquad (2.4\mathrm{b})$$

$$\nabla^2\vartheta - R\Delta_2\varphi = (\boldsymbol{\delta}\varphi + \boldsymbol{\varepsilon}\psi)\cdot\nabla\vartheta + (U\partial_x + \partial_t)\vartheta . \qquad (2.4\mathrm{c})$$

In addition an equation is needed for the component $U^{(x)}$ of the mean velocity field,

$$(\partial^2_{zz} - \partial_t)U^{(x)} + \partial_z[\overline{\Delta_2\varphi(\partial^2_{xz}\varphi + \partial_y\psi)}] + \bar{\vartheta}\tan\gamma = 0 , \qquad (2.4\mathrm{d})$$

where the bar indicates the average over the x, y-plane. The symbol Δ_2 has been introduced for $\nabla^2 - \partial^2_{zz}$ and P is the Prandtl number, $P = \nu/\kappa$. The boundary conditions for φ, ψ, ϑ and $U^{(x)}$ are given by

$$\varphi = \partial_z\varphi = \psi = \vartheta = U^{(x)} = 0 \quad \text{at } z = \pm\frac{1}{2} . \qquad (2.5)$$

Longitudinal rolls corresponding to x-independent steady solutions of the problem (2.4), (2.5) and their instabilities have been investigated in CB77. The variables φ, ϑ describing longitudinal rolls are the same as in a horizontal layer. The parameter γ only enters the solution for ψ and $U^{(x)}$; the convective heat transport as a function of the Rayleigh number as defined by (2.2) is thus independent of γ. The main instability of longitudinal rolls is the wavy instability which is the origin of some of the three-dimensional forms of convection observed in the experiments by Hart (1971), Ruth et al. (1980a) and others. The following analysis is devoted to the study of finite amplitude properties of this type of convection.

Since the imaginary part of the growth rate of the wavy instability vanishes we expect an evolution of the instability towards a steady three-dimensional solution of equations (2.4). Using the Galerkin method we expand the variables φ, ψ, ϑ and $U^{(x)}$ into complete systems of functions satisfying the boundary conditions (2.5),

$$\varphi = \sum_{\lambda,\mu,\nu} a_{\lambda\mu\nu} \begin{Bmatrix} \cos \lambda\alpha_x x \\ \sin \lambda\alpha_x x \end{Bmatrix} g_\nu(z)[p(\lambda)\cos\mu\alpha_y y + (1-p(\lambda))\sin\mu\alpha_y y]\,, \tag{2.6a}$$

$$\psi = \sum_{\lambda,\mu,\nu} c_{\lambda\mu\nu} \begin{Bmatrix} \cos \lambda\alpha_x x \\ \sin \lambda\alpha_x x \end{Bmatrix} \sin \nu\pi(z + \tfrac{1}{2})[p(\lambda)\sin\mu\alpha_y y + (1-p(\lambda))\cos\mu\alpha_y y]\,, \tag{2.6b}$$

$$\vartheta = \sum_{\lambda,\mu,\nu} b_{\lambda\mu\nu} \begin{Bmatrix} \cos \lambda\alpha_x x \\ \sin \lambda\alpha_x x \end{Bmatrix} \sin \nu\pi(z + \tfrac{1}{2})[p(\lambda)\cos\mu\alpha_y y + (1-p(\lambda))\sin\mu\alpha_y y]\,, \tag{2.6c}$$

$$U^{(x)} = \sum_\nu U_{1\nu} \sin 2\nu\pi(z + \tfrac{1}{2})\,, \tag{2.6d}$$

where the summation runs through positive integers ν and non-negative integers λ and μ and where the function $p(\lambda)$,

$$p(\lambda) = 1 \quad \text{for even } \lambda\,, \qquad p(\lambda) = 0 \quad \text{for odd } \lambda \tag{2.7}$$

has been introduced in order to capture the symmetry of the convection flow generated by the interaction of the wavy instability with the longitudinal rolls. Another aspect of this symmetry manifests itself in the selection rule that the upper function in the wavy bracket must be chosen for even $\nu + \mu$ and the lower function for odd $\nu + \mu$. The functions $g_\nu(z)$ were first introduced by Chandrasekhar (1961, p. 635) and are also defined in CB77. After introducing the representations (2.6) into equations (2.4), multiplying the equations by the respective expansion functions and averaging them over the fluid layer, we obtain a system of nonlinear algebraic equations for the coefficients $a_{\lambda\mu\nu}$, $c_{\lambda\mu\nu}$, $b_{\lambda\mu\nu}$, $U_{1\nu}$. After truncating this infinite system of equations it can be solved by a Newton–Raphson method. As in the case of similar problems (Clever and Busse, 1987, 1989) the truncation condition in which all coefficients and corresponding equations satisfying

$$\lambda + \mu + \nu > N_T$$

are dropped offers an optimal combination of computational efficiency and economy. Almost all computations to be reported in the following have been carried out for $N_T = 6, 8$ and 10. In the plots the results obtained for $N_T = 10$ are shown provided they differ by less than a few percent from those obtained for $N_T = 8$. Only at the highest values of R $N_T = 12$ has also been used.

The Galerkin method offers the opportunity for a relatively simple analysis of the stability of the steady three-dimensional solutions. Arbitrary infinitesimal disturbances can be superimposed onto the steady solution and their growth rate can be determined. Here we shall restrict the analysis to those disturbances which fit the x, y-periodicity interval of the steady solution. This procedure excludes disturbances with finite Floquet exponents which are usually of lesser importance. The main reason for this restriction is that disturbances which fit the periodicity interval of the steady solution can be separated into four subsets differing in their symmetries with respect to the steady solution. This separation facilitates

the stability analysis enormously since the eigenvalues of much smaller matrices must be evaluated. The infinitesimal disturbances that we are considering can thus be represented in the form

$$\tilde{\varphi} = \sum_{\lambda,\mu,\nu} \tilde{a}_{\lambda\mu\nu} \begin{Bmatrix} \cos \lambda\alpha_x x \\ \sin \lambda\alpha_x x \end{Bmatrix} g_\nu(z) [\tilde{p}(\lambda) \cos \mu\alpha_y y + (1 - \tilde{p}(\lambda)) \sin \mu\alpha_y y] \exp(\sigma t) , \tag{2.8a}$$

$$\tilde{\psi} = \sum_{\lambda,\mu,\nu} \tilde{c}_{\lambda\mu\nu} \begin{Bmatrix} \cos \lambda\alpha_x x \\ \sin \lambda\alpha_x x \end{Bmatrix} \sin \nu\pi(z + \tfrac{1}{2}) [\tilde{p}(\lambda) \sin \mu\alpha_y y + (1 - \tilde{p}(\lambda)) \cos \mu\alpha_y y] \exp(\sigma t) ,$$
$$\tag{2.8b}$$

$$\tilde{\vartheta} = \sum_{\lambda,\mu,\nu} \tilde{b}_{\lambda\mu\nu} \begin{Bmatrix} \cos \lambda\alpha_x x \\ \sin \lambda\alpha_x x \end{Bmatrix} \sin \nu\pi(z + \tfrac{1}{2}) [\tilde{p}(\lambda) \cos \mu\alpha_y y + (1 - \tilde{p}(\lambda)) \sin \mu\alpha_y y] \exp(\sigma t) ,$$
$$\tag{2.8c}$$

$$\tilde{U}^{(x,y)} = \sum_\nu \hat{p}(\nu) \tilde{U}_\nu^{(x,y)} \sin \nu\pi(z + \tfrac{1}{2}) \exp(\sigma t) , \tag{2.8d}$$

where the four classes *SE*, *SO*, *AE*, *AO* can be distinguished according to the following definitions:

$$S: \ \tilde{p}(\lambda) = p(\lambda) , \qquad A: \ \tilde{p}(\lambda) = 1 - p(\lambda) , \tag{2.9a}$$

E(O): Upper (lower) functions in the wavy brackets correspond to even $\nu + \mu$ and lower (upper) functions correspond to odd $\nu + \mu$. $\qquad\qquad$ (2.9b)

The disturbance mean flow (2.8d) for the classes S is directed solely in the x-direction, while for the classes A only a disturbance mean flow in the y-direction can exist. The mean flows are symmetric (antisymmetric) with respect to the plane $z = 0$ in the classes *SO* and *AE* (*SE* and *AO*). Accordingly $\hat{p}(\nu) = p(\nu)$ holds for *SO* and *AE* and $\hat{p}(\nu) = 1 - p(\nu)$ for *SE* and *AO*.

3. Steady three-dimensional convection flows

Three-dimensional solutions of the form (2.6) have been obtained for a variety of Prandtl numbers and angles of inclinations. The wavenumber α_y has been fixed at the critical value $\alpha_c = 3.117$ for the onset of longitudinal convection rolls because those rolls remain stable up to the Rayleigh number R_{II} for the onset of the wavy instability. Once the threshold value R_{II} is exceeded, wavy roll solutions exist for a broad band of wavenumbers α_x. Since the value α_x of the strongest growing disturbance increases significantly with R beyond the threshold value R_{II} according to CB77 and since typical observations (Hart, 1971) of experimentally realized wavy rolls exhibit relatively large values of α_x, we have chosen values of α_x which appear to be representative for the wavy roll regime.

For all cases that have been studied, the transition from longitudinal rolls to wavy rolls causes a drop in the convective heat transport. A typical example can be seen in Fig. 2 in which results for the case of Prandtl number $P = 12$ have been plotted. There thus exists a region for which the Nusselt number decreases with increasing Rayleigh number. For lower
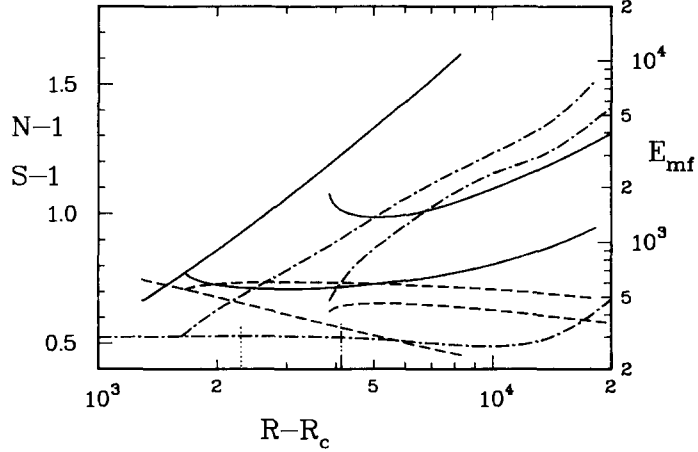
Fig. 2. Nusselt number N (solid lines), shear Nusselt number S (dashed lines) and kinetic energy of the mean flow E_{mf} (dash-dotted lines) for longitudinal rolls and wavy rolls with $\alpha_x = 1.5$ (bifurcating at $R - R_c \simeq 1.6 \cdot 10^3$) and with $\alpha_x = 2.0$ starting at about $R - R_c = 3.8 \cdot 10^3$. The wavy rolls become unstable at the Rayleigh numbers indicated by short lines (dotted for $\alpha_x = 1.5$, dash-double-dotted for $\alpha_x = 2.0$). The parameters $P = 12$, $\gamma = 60°$, $\alpha_y = 3.117$ have been assumed.

Prandtl numbers this effect is less pronounced, but the growth of the Nusselt number is always reduced in comparison with the case of longitudinal rolls.

In analogy to the Nusselt number N which is defined as the ratio of the heat transport with and without convection, the shear Nusselt number S can be defined as the ratio of the shear stresses at the walls in the presence and in the absence of convection,

$$S \equiv \left[\frac{\partial}{\partial z} U \bigg/ \frac{\partial}{\partial z} U_0 \right]_{z = \pm \frac{1}{2}}. \tag{3.1}$$

Longitudinal convection rolls are very effective in reducing the shear stress primarily because an effective heat transport decreases the mean temperature gradient in the interior of layer which is responsible for driving the cubic profile flow. It is thus not surprising that an increase of S occurs together with a decrease of N. The kinetic energy of the mean flow,

$$E_{mf} \equiv \tfrac{1}{2} \langle U^2 \rangle \tag{3.2}$$

also increases with the onset of wavy rolls. Here the angular brackets indicate the average over the fluid layer.

Another interesting effect that can be seen in Fig. 2 is the subcritical onset of wavy rolls for larger values of α_x, say $\alpha_x \gtrsim 2$. Because on the inverted part of the solution branch the numerical scheme does not converge, the three-dimensional solution in the case $\alpha_x = 2.0$ is not connected in the figure with a bifurcation point on the longitudinal roll solution. The numerical scheme mimics the physical system in this respect since the inverted part of the bifurcating branch can also not be realized because of its instability.

In Fig. 3 the kinetic energies of the fluctuating components of the velocity field are shown which are defined by

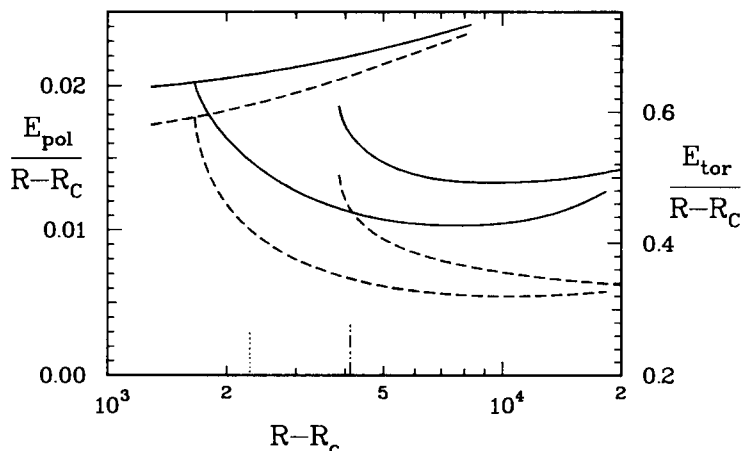$$E_{pol} \equiv \tfrac{1}{2} \langle |\nabla \times (\nabla \times \mathbf{k}\varphi)|^2 \rangle , \tag{3.3a}$$

Fig. 3. Same as in Fig. 2 except that E_{pol} (solid lines) and E_{tor} (dashed lines) have been plotted.

$$E_{\text{tor}} \equiv \tfrac{1}{2} \left\langle \left| \nabla \times \mathbf{k}\psi \right|^{2} \right\rangle . \tag{3.3b}$$

As is evident from the figure, these quantities increase roughly in proportion to $R - R_c$ for longitudinal rolls, but vary much less rapidly with R after the onset of wavy rolls.

In Figs 4 through 6 results for water ($P = 7$) are shown for two different angles of inclination. The change in the heat transport caused by the onset of wavy rolls is less dramatic than in the case $P = 12$ and a tendency towards a recovery of the transport efficiency can be noticed at higher Rayleigh numbers. This latter tendency is especially pronounced at the high inclination of $\gamma = 80°$ where it has also been found that the energy of the poloidal component of flow can grow to values much higher than the corresponding values of longitudinal rolls. This result may indicate a tendency towards the realisation of transverse rolls which are a strong competitor for longitudinal rolls at high inclinations according to linear theory.
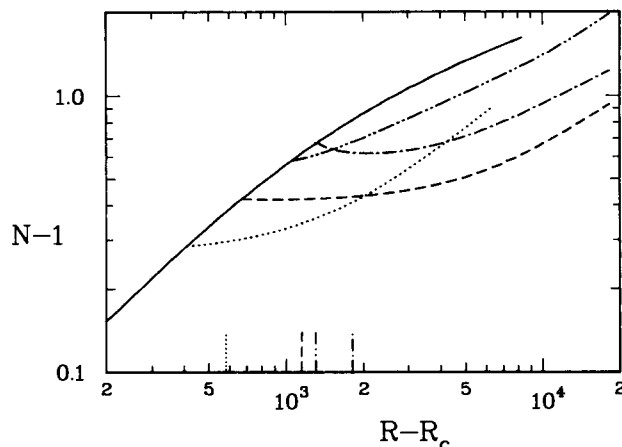
Fig. 4. Nusselt number N in the case $P = 7$, $\alpha_y = 3.117$ for longitudinal rolls (solid line) and wavy rolls with $\alpha_x = 1.5$ (dashed line) and $\alpha_x = 2.0$ (dash-dotted) for $\gamma = 60°$ and with $\alpha_x = 1.5$ (dotted) and $\alpha_x = 2.0$ (dash double-dotted) for $\gamma = 80°$. The Rayleigh numbers at which the respective wavy rolls become unstable are indicated at the abscissa.
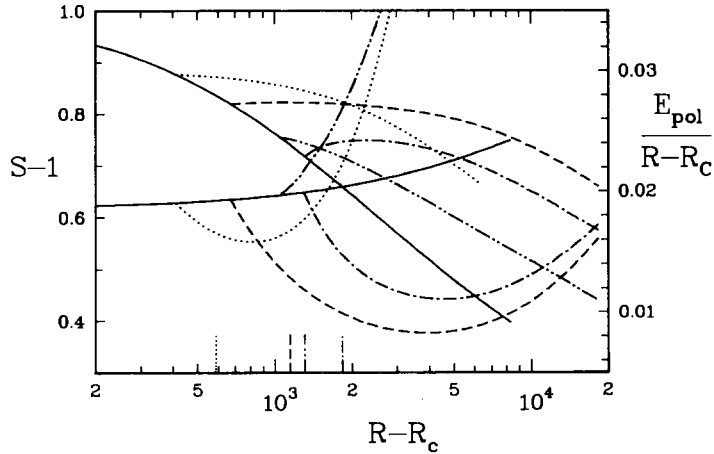
Fig. 5. Shear Nusselt numbers (descending solid line and attached branches) and E_{pol} for the same cases as in Fig. 4.

While the Prandtl number of water at room temperature is 7, it decreases rapidly with increasing temperature and reaches a value of about 2.5 at 60°C. This property has motivated the computations for the case $P = 2.5$ displayed in Figs 7 and 8. It is evident from these figures that the results resemble qualitatively those obtained in the higher Prandtl number cases. Since the difference $R_{II} - R_c$ between the thresholds for wavy rolls and longitudinal rolls increases almost proportional to P^2 according to Fig. 10 of CB77, the curves shown in Figs 7 and 8 are shifted to much lower values of R in comparison to those of the previous figures.

Because of the general similarity of the evolution of wavy rolls for different values of γ and P, we show only a few representative plots of the flow structure. The left-hand column of Fig. 9 shows the relatively smooth dependence of the flow field in the case of lower inclination, lower Prandtl number, and lower Rayleigh number, while all of these parameters assume higher values in the case of the right-hand column, where much smaller flow structures become visible. It is remarkable that the isotherms are almost identical to the lines
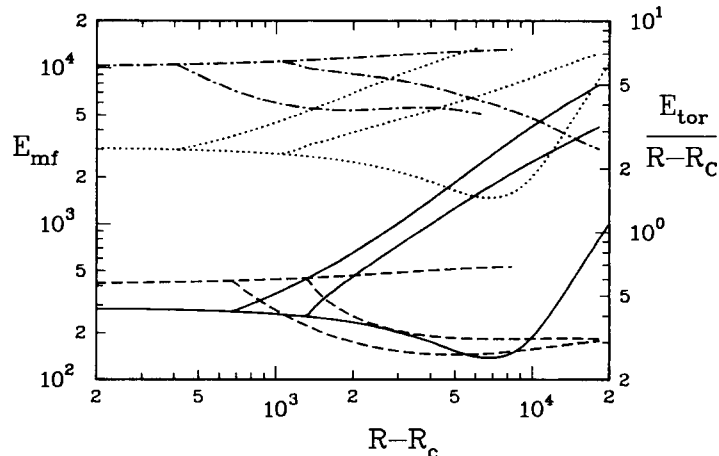

Fig. 6. E_{mf} (solid lines for $\gamma = 60°$, dotted lines for $\gamma = 80°$) and E_{tor} (dashed lines for $\gamma = 60°$, dash-dotted lines for $\gamma = 80°$) for the same parameter values as in Fig. 4.
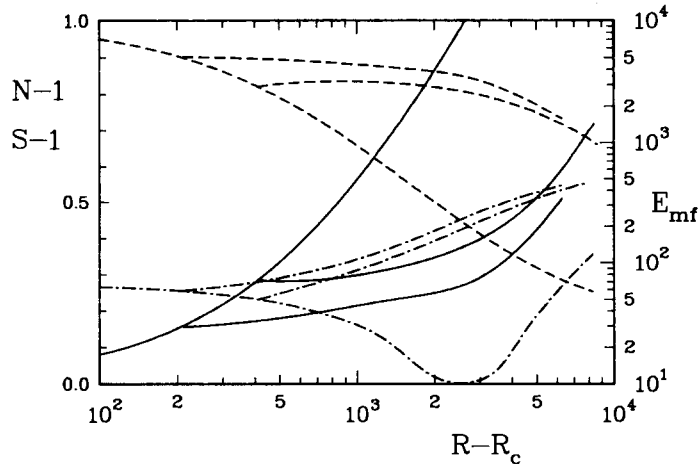
Fig. 7. Nusselt number N (solid lines), shear Nusselt number S (dashed lines), and E_{mf} (dash-dotted) for longitudinal rolls and for bifurcating wavy rolls with $\alpha_x = 1.5$ (bifurcating at $R - R_c \simeq 200$) and with $\alpha_x = 2.0$ in the case $P = 2.5$, $\gamma = 40°$, $\alpha_y = 3.117$.

of constant velocity in the z-direction in the case of lower Prandtl numbers. While lines of positive and negative z-velocity exhibit the expected symmetry in the center plane, $z = 0$, a considerable asymmetry develops as one moves to planes closer to the boundaries. The plots in the middle of the figure exhibit this property quite clearly. The features of wavy rolls in the case $P = 2.5$ are also visible in the case of $P = 0.71$ shown in Fig. 10. In addition, the toroidal component of the velocity has been plotted in this figure which shows the effect of the advection of mean flow by the z-component of the velocity field.

Figures 11 through 15 display results obtained for an inclined air layer ($P = 0.71$). In Fig. 11 the Nusselt number is plotted for a number of different values of γ and α_x. It is interesting to see, that the recovery of the Nusselt number for wavy rolls to values comparable to those of longitudinal rolls is almost complete in the case $\gamma = 25°$. But at higher angles of inclination the Nusselt number deficiency for wavy rolls persists. The change of the shear Nusselt number S induced by wavy rolls and plotted in Fig. 12 is even more dramatic than at the
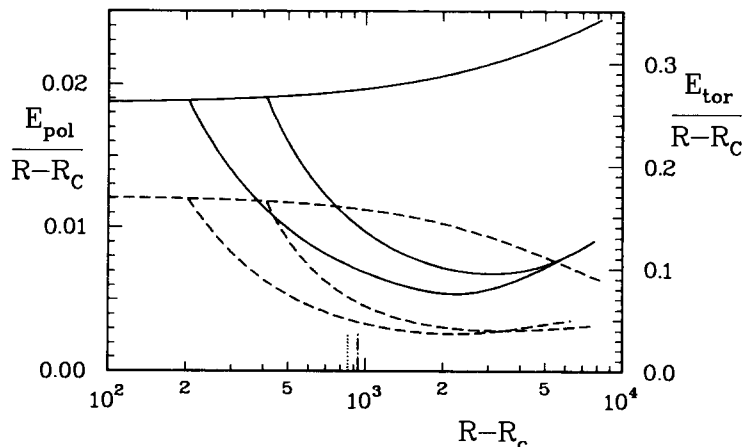

Fig. 8. E_{pol} (solid lines) and E_{tor} (dashed lines) for the same parameter values as in Fig. 7. The Rayleigh numbers at which the wavy rolls become unstable are indicated at the abscissa (dotted for $\alpha_x = 1.5$, dash-dotted for $\alpha_x = 2.0$).
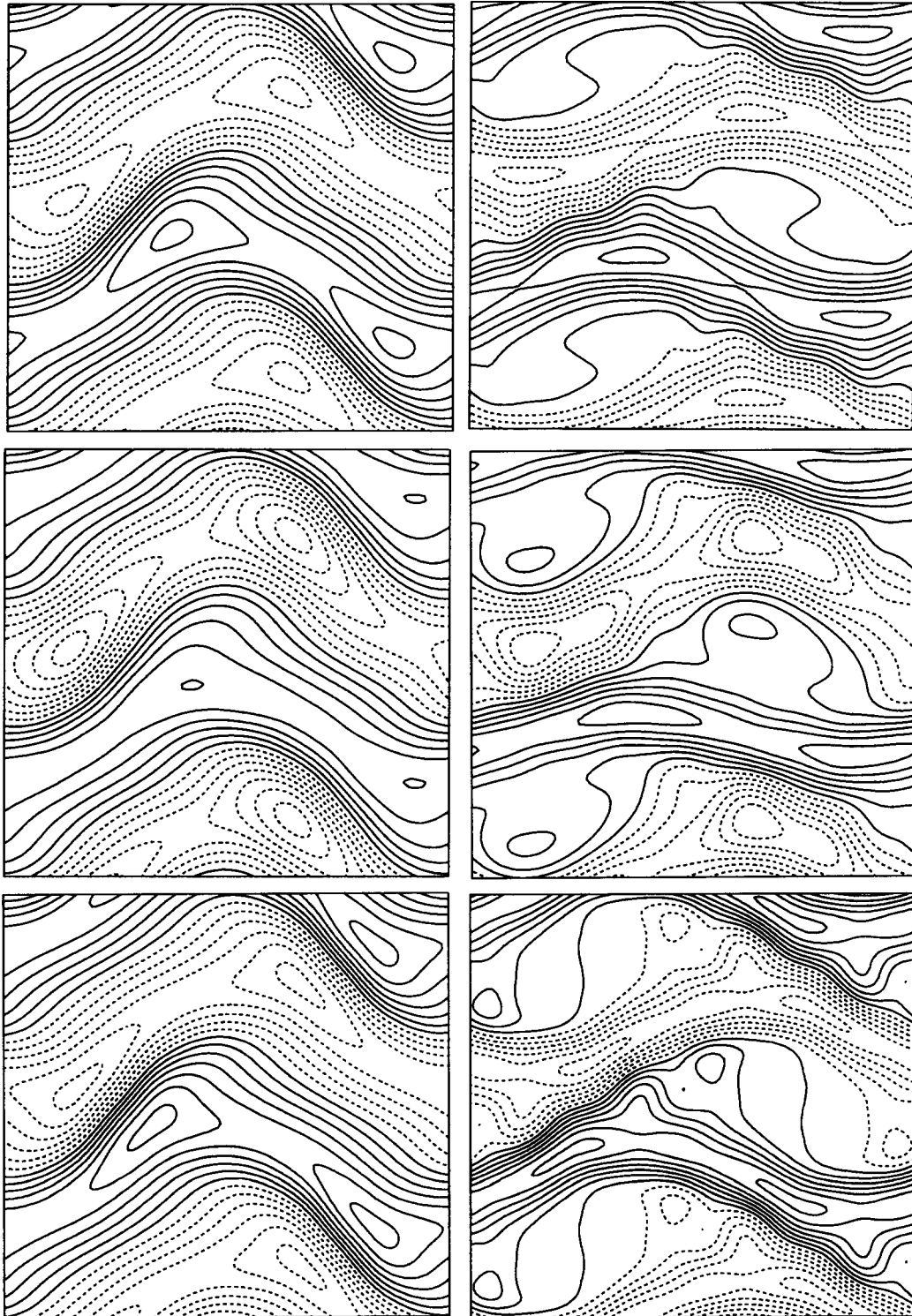
Fig. 9. Lines of constant normal velocity, $-\Delta_2\varphi = $ const., in the planes $z = 0$ (top row) and $z = -0.3$ (middle row) and isotherms in the plane $z = 0$ (bottom row) for the cases $P = 2.5$, $\gamma = 40°$, $R = 3500$ (left column) and $P = 7$, $\gamma = 60°$, $R = 10^4$ (right column). $\alpha_x = 2.0$, $\alpha_y = 3.117$ and $N_T = 10$ have been used in all cases. Solid lines describe positive values, dashed lines correspond to negative values and solid line adjacent to the dashed lines indicates zero. The y-direction is upward, the x-direction towards the right.
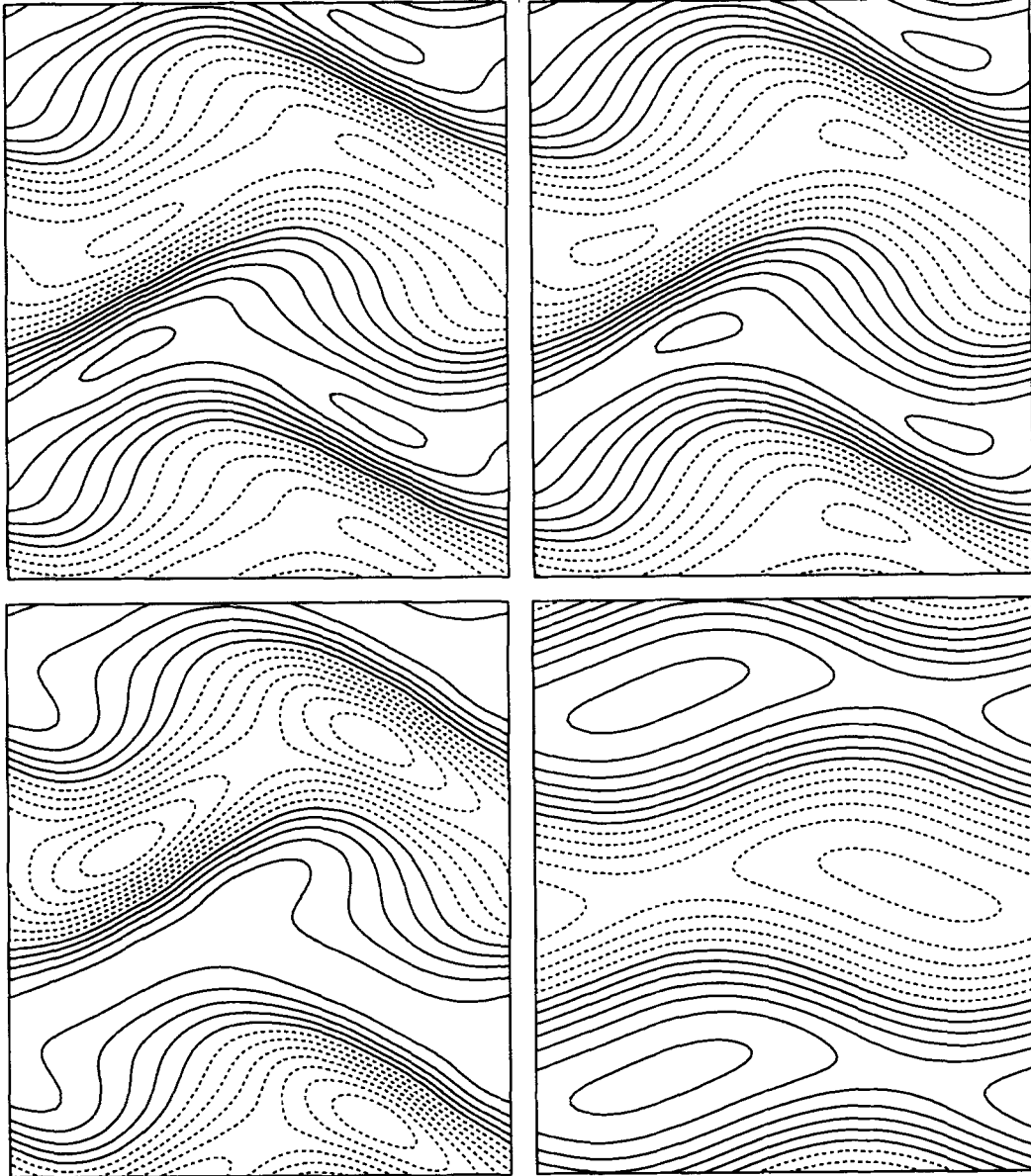
Fig. 10. Lines of constant normal velocity, $-\Delta_2\varphi = $ const., in planes $z = 0$ (upper left) and $z = -0.3$ (lower left), isotherms in the plane $z = 0$ (upper right) and streamlines of the toroidal component of the velocity field, $\psi = $ const., in the plane $z = 0$ (lower right) for $P = 0.71$, $R = 2490$, $\gamma = 40°$, $\alpha_x = 2.4$, $\alpha_y = 3.117$. Solid (dashed) lines indicate positive (negative) values and the solid line adjacent to the dashed lines describes zero. The y-direction is upward, the x-direction towards the right.

higher Prandtl numbers mainly because the decrease of S with increasing R owing to the actions of longitudinal rolls becomes more pronounced at lower Prandtl numbers. The changes in the energies of the fluctuating and of the mean velocity fields shown in Figs 13 through 15 are very similar to those found in the case of higher Prandtl numbers except for a shift owing to the strong dependence of R_{II} on P which we have mentioned above.

In the last two Figs 16 and 17, profiles of the mean flow $U(z)$ are shown. The amplitude of mean flow is reduced in comparison with the cubic profile flow (2.1b), but not as much as in
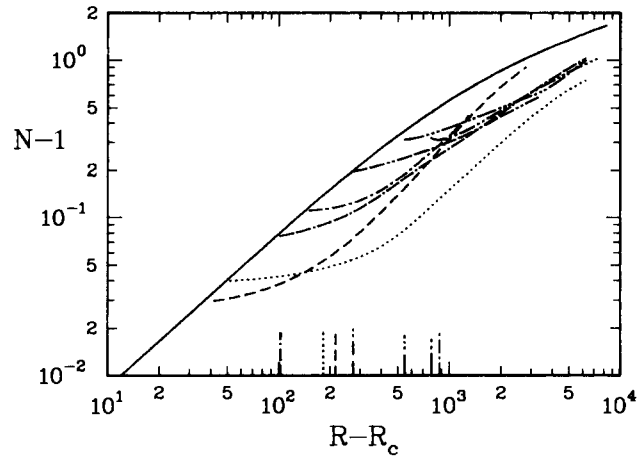
Fig. 11. Nusselt number N for longitudinal rolls (solid line) and wavy rolls with $\alpha_x = 1.5$ (dashed line) and $\alpha_x = 2.1$ (dash-dotted) for $\gamma = 25°$, with $\alpha_x = 1.5$ (dotted line) and $\alpha_x = 2.4$ (dash double-dotted) for $\gamma = 40°$, and with $\alpha_x = 1.2$ (double-dash-dotted), $\alpha_x = 1.8$ (double-dash double-dotted) and $\alpha_x = 2.1$ (dash triple-dotted) for $\gamma = 60°$. The parameters $P = 0.71$ and $\alpha_y = 3.117$ have been assumed. The Rayleigh numbers at which the respective wavy rolls become unstable have been indicated at the abscissa.
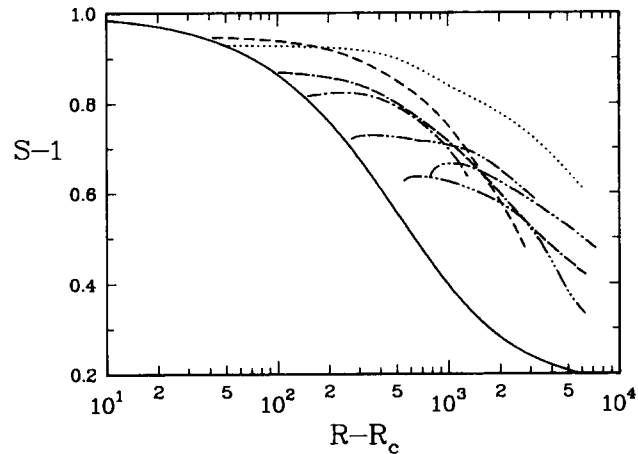

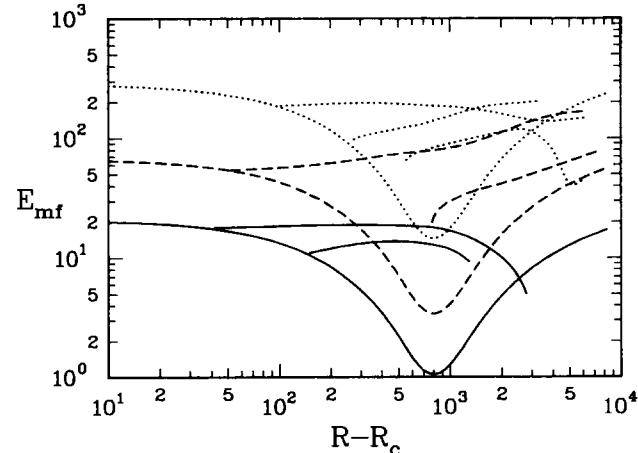*Fig. 12.* Same as Fig. 11 for the shear Nusselt number.

Fig. 13. Kinetic energy of the mean flow E_{mf} for longitudinal rolls and bifurcating solutions of wavy rolls in the cases $\gamma = 25°$ (solid lines), $\gamma = 40°$ (dashed lines), and $\gamma = 60°$ (dotted lines). The parameter values are the same as in Fig. 11.

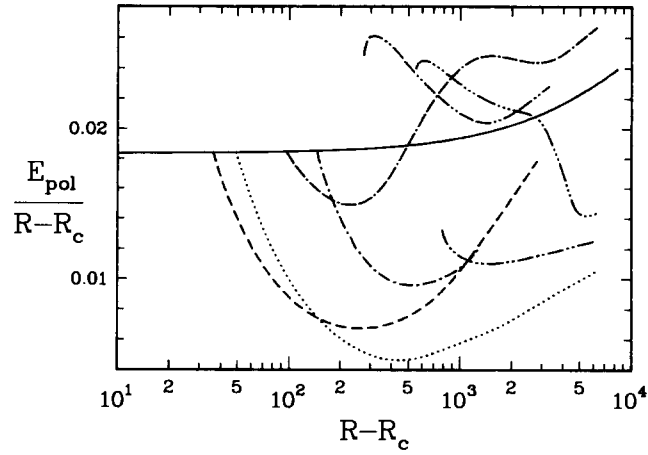*Fig. 14.* Same as Fig. 11 for $E_{pol}/(R - R_c)$ instead of $N - 1$.

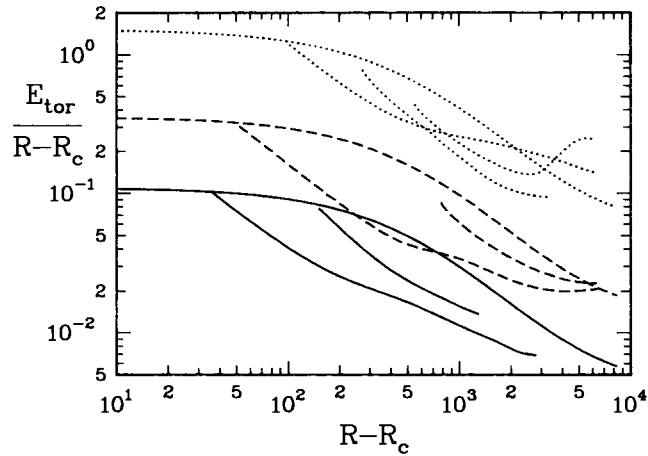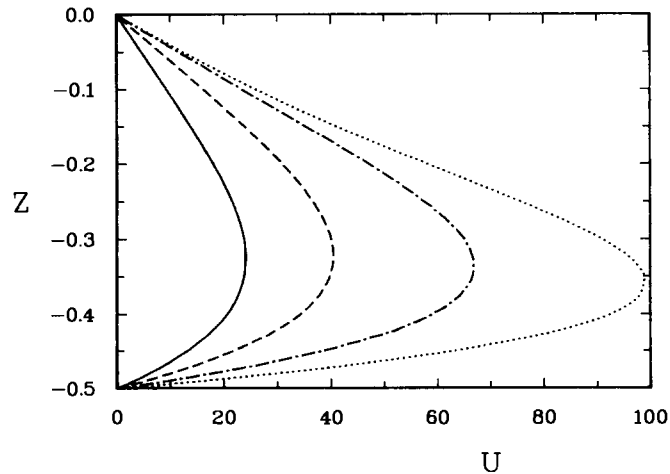*Fig. 15.* Same as Fig. 13 for $E_{tor}/(R - R_c)$ instead of E_{mf}.

Fig. 16. Mean flow profile $U(z)$ for wavy convection rolls in an inclined layer with $P = 7$, $\gamma = 60°$, $\alpha_x = 2.1$, $\alpha_y = 3.117$. The curves correspond (left to right) to $R = 3100$, 5000, 10^4, $2 \cdot 10^4$.
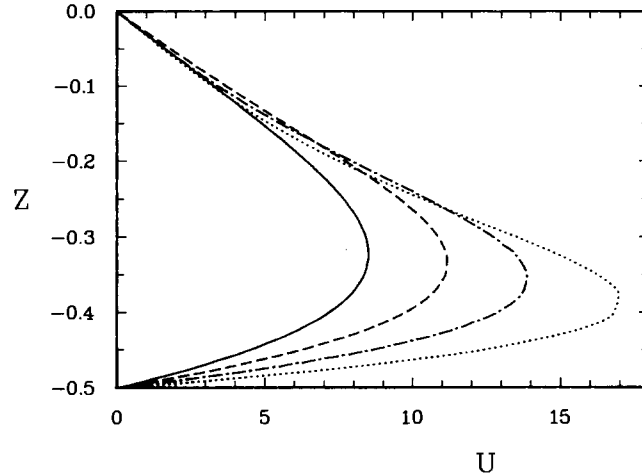
Fig. 17. Same as Fig. 16, but for $P = 0.71$, $\gamma = 40°$. The curves correspond to $R = 2000$ (solid), 3000 (dashed), 5000 (dash-dotted), 10^4 (dotted).

the case of longitudinal rolls (see Figs 3 and 4 of CB77 for comparison). The maximum of mean flow profile is shifted towards the boundary with increasing Rayleigh number since the x, y-average of the temperature in the interior of the layer becomes nearly isothermal and the buoyancy force driving the mean flow becomes located in the thermal boundary layers. As must be expected from the Prandtl number dependence of equations (2.4), the convection induced effects on the mean flow are much more dramatic in the case of air than in the case of water.

4. Instabilities of wavy convection rolls

The procedure for the search of growing disturbances has been outlined at the end of Section 2. Growth rates σ have been obtained for all four classes of disturbances SE, SO, AE, AO. The results of the computations show that disturbances of the class SE, usually yield the highest real part σ_r of σ for $P \gtrsim 1$. In the case of air, $P = 0.71$, disturbances of the classes SE, AE and AO are close competitors and for $P = 0.3$ AO disturbances dominate.

The instability in the case $P \gtrsim 1$ always exhibits a finite imaginary part σ_i of the growth rate. The period corresponding to the frequency σ_i appears to be roughly related to the circulation time in the rolls. Because the growing disturbances do not change the symmetry of the steady wavy roll solution, it is relatively easy to follow its evolution by a forward integration in time. For this purpose the coefficients a_{lmn}, b_{lmn} c_{lmn} in expressions (2.b) are assumed to be functions of time and a Crank–Nicholson scheme is used for the numerical integration. After transients have died away it is found that a periodic oscillation occurs in which the flow appears to vacillate between the state of longitudinal rolls and a state of nearly transverse oriented vortices as is evident from the example shown in Fig. 18. The mean quantities plotted as a function of time in Fig. 18a are periodic with half the period of oscillation as can be seen from the comparison with the flow field shown in Fig. 18b. The interval of growing transport of heat and momentum corresponds to the state of nearly aligned longitudinal rolls. In the sudden transition to modulated transverse vortices kinetic energy of the toroidal component is converted into kinetic energy of the poloidal component
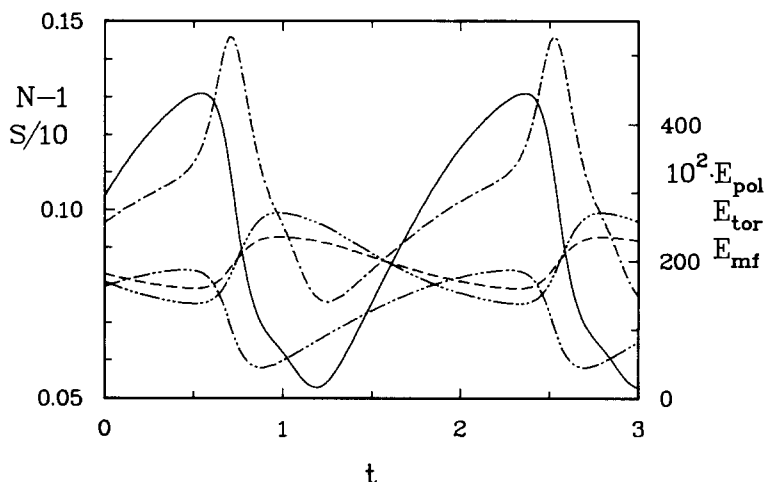
Fig. 18a. The Nusselt number N (solid line), the shear Nusselt number S (dashed), the kinetic energies of the poloidal (dash-dotted), toroidal (dash double-dotted) and mean (dash triple-dotted) components of the velocity field as a function of time for vacillating convection with $R = 1900$, $P = 0.71$, $\gamma = 60°$, $\alpha_x = 1.2$, $\alpha_y = 3.117$.

of the velocity field. But since the longitudinal orientation of the rolls is lost, the transports are decreased in this process. After the decay of the modulated transverse vortices the longitudinal rolls start to grow again.

Since the cases where the vacillation instability occurs are also characterized by relatively high angles of inclination where the critical Rayleigh numbers for the onset of longitudinal rolls and for transverse vortices get relatively close, the vacillation between these two states is perhaps not surprising. It must be taken into account in this connection that two-dimensional transverse vortices are not very stable according to the analysis of Nagata and Busse (1983) and that they are replaced by three-dimensional vortices exhibiting significant structure in the transverse direction similar to that of the second picture from the top of Fig. 18b in the middle column.

While wavy rolls in an air layer with 40° inclination and $\alpha_x \geq 1.8$ are unstable with respect to the vacillation instability, the instability with the AO symmetry and with vanishing σ_i predominates at lower angles of inclination and low values of α_x, $\alpha_x \leq 1.5$. For intermediate cases such as $\gamma = 25°$, $\alpha_x = 2.1$ and $\gamma = 40°$, $\alpha_x = 1.5$ the preferred instability is of the AE-type. As is evident from Fig. 11, the region in which wavy rolls are stable in the case of 25° inclination is so small that we feel forced to conclude that the wavy rolls observed in the experiments of Ruth et al. (1980a) are not the original wavy rolls analyzed in this paper, but they are instead those which are already modified by the AE-type instability which appears to be most relevant for the parameters of the experiment. Obviously the effects of this modification are not very dramatic since the observed convection exhibits a close resemblance to wavy rolls. Consistent with this interpretation is the fact that Ruth et al. report slight lateral motions whenever the angle of inclination reaches a value $\gamma \geq 20°$. This property must be expected in the case of an AE-type instability according to the discussion at the end of Section 2.

In order to test this hypothesis, we have done a forward integration in time in the case $\gamma = 40°$, $\alpha_x = 1.5$, $\alpha_y = 3.117$, $R = 2000$. Since the number of coefficients that must be determined as function of time is twice the number for steady wavy rolls due to symmetry considerations, the computations become rather time consuming. The remarkable result that
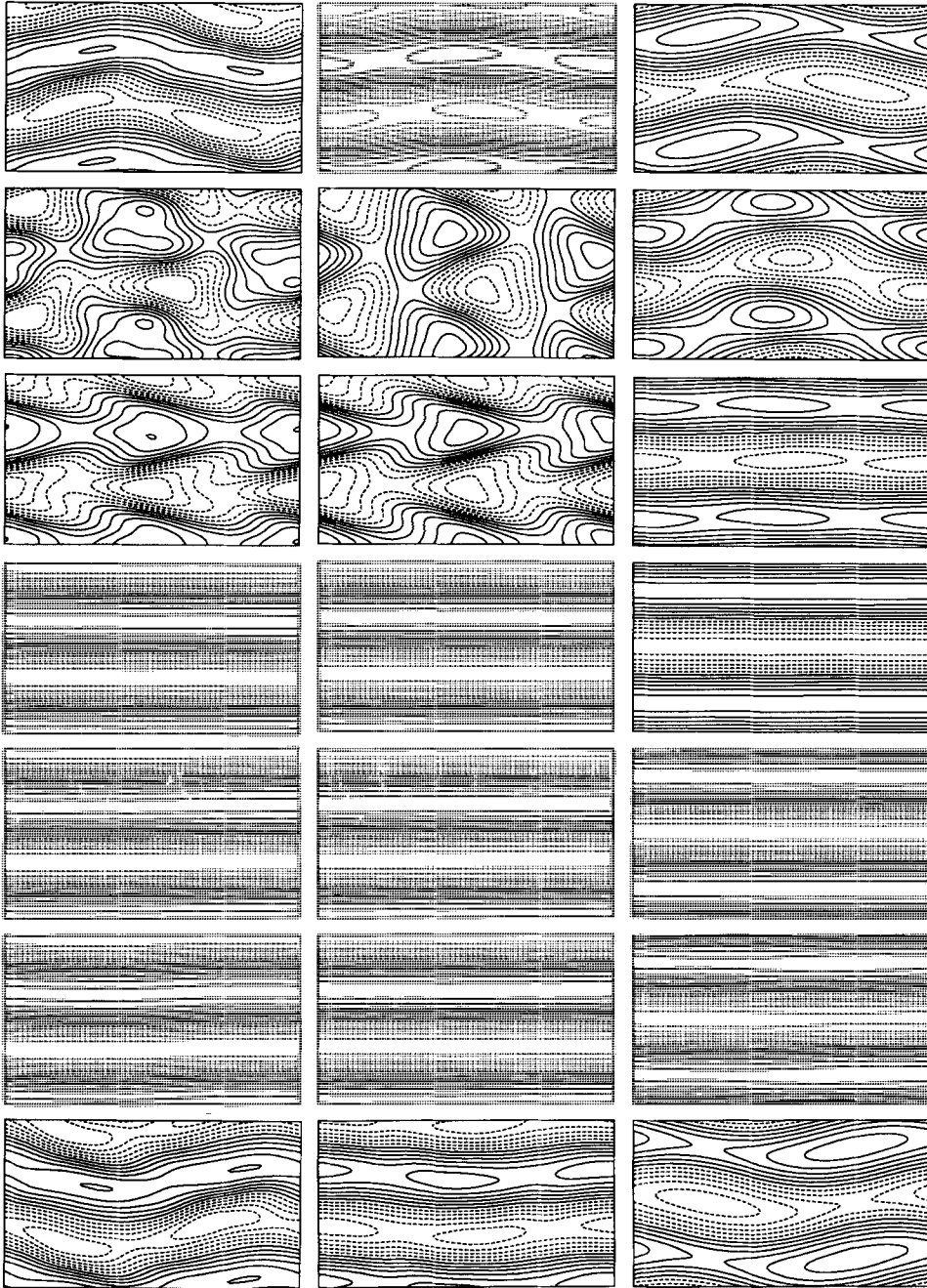
Fig. 18b. Lines of constant normal velocity at $z = -0.3$ (left column) and at $z = 0$ (middle column) and lines of constant ψ at $z = 0$ (right column) are shown at equal time steps ($\Delta t = 0.3034$) starting at the time 0.585 of Fig. 18a such that half a cycle is completed at the time 2.405 corresponding to the bottom row. Solid (dashed) lines indicate positive (negative) values except for the solid line adjacent to the dashed lines which indicates zero. The y-direction is upward, the x-direction towards the right. Parameter values are the same as in Fig. 18a.
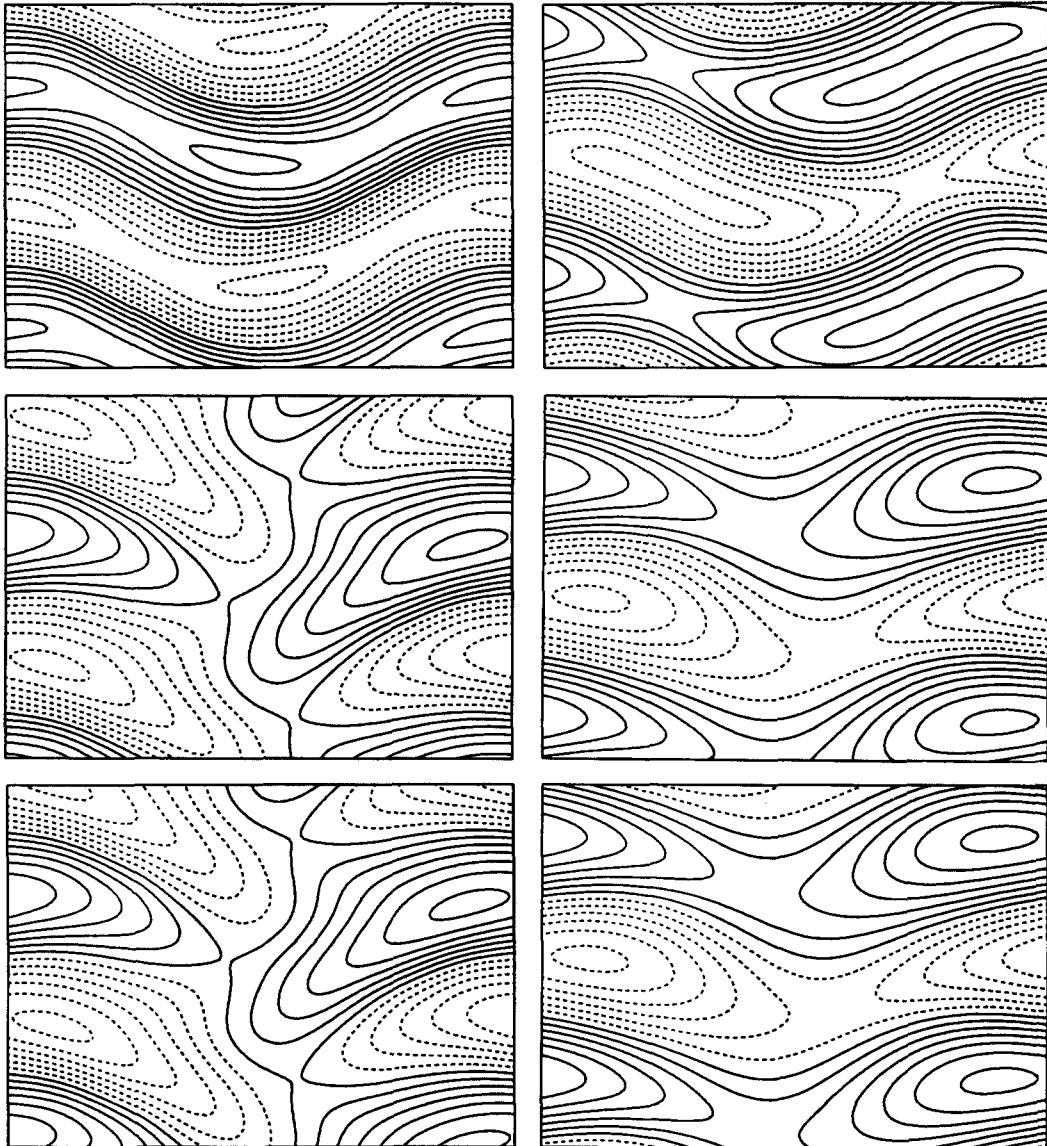
Fig. 19. Lines of constant velocity u_z (left column) and constant toroidal stream function ψ (right) in the plane $z = 0$ for steady wavy rolls (top row) and for drifting asymmetric wavy rolls (middle and bottom rows) at two points in time, $\Delta t = 1.0$ apart. The parameter values $R = 2000$, $P = 0.71$, $\gamma = 40°$, $\alpha_x = 1.5$, $\alpha_y = 3.117$, $N_T = 8$ have been used.

has been found is displayed in Fig. 19. The growing disturbances do indeed change the original wavy roll pattern. But after a short transient, a stationary pattern of asymmetric wavy rolls is again attained except for a constant drift in the transverse direction. This direction depends on the sign of the critical disturbances of AE-type. Thus, left or right drifting patterns can be obtained, depending on the choice of initial conditions.

5. Concluding discussion

Although the problem of inclined layer convection has received considerable attention from experimenters, there exist few opportunities for a quantitative comparison of the theoretical results of this paper with laboratory observations. The general result that less heat is transported by wavy rolls than by longitudinal rolls is borne out by the experimental data of Ruth et al. (1980a). For a more detailed discussion of the heat flux data see Ruth et al. (1980b). But a quantitative comparison between theory and experiment is difficult for a number of reasons. First, the finite extent of experimental layers causes end effects and leads to a longitudinal component of the temperature gradient in the basic state which exerts a considerable influence on the dynamics of the system (Hart, 1971; Bergholz, 1978). Second, the finite lateral extent of the layer and its influence on the mean flow are not represented in the theory. The finite conductivity of the bounding surfaces of the enclosed fluid and deviations from the Boussinesq approximation also can give rise to asymmetries which may cause discrepancies between theory and experiment. For instance, the stationarity of wavy rolls which depends on the antisymmetry of the mean flow with respect to the center plane of the layer will give way to a time dependence once this symmetry is broken.

A detailed discussion of the problem of convection in inclined enclosures can be found in the book by Schinkel (1980) who also presents new theoretical and experimental results for the case of inclined rectangular boxes of finite aspect ratio filled with air. The theoretical computations are restricted, however, to the case of two-dimensional transverse rolls. Three-dimensional solutions for wavy patterns are described in the present paper for the first time. While finite aspect ratios and deviations from the Boussinesq approximation will undoubtedly affect quantitative aspects of these solutions, they clearly represent the wavy structure seen in experiments as demonstrated by the close similarity between the photographs of Hart (1971) and the plots of Figs 9 and 10. The analysis of the time-dependent three-dimensional solutions which bifurcate from the wavy rolls according to stability analysis are of special interest. The few preliminary cases that we have reported in this paper have already exhibited a number of unexpected features and a more systematic study appears to be warranted. Perhaps those surprising features such as the vacillations and the transverse drift will stimulate new experimental investigations.

The findings of this paper may have implications for the design of solar heat collectors. The presence of convection in an inclined layer strongly reduces the mean circulation which transports a considerable amount of heat in inclined layers of finite extent. Secondly, the heat transport by wavy rolls is much reduced in comparison with longitudinal rolls. It may thus be advantageous to realize the Rayleigh number regime where both the Nusselt number and mean flow strength are relatively low.

References

Bergholz, R.F., Instabilities of steady natural convection in a vertical fluid layer. *J. Fluid Mech.* 84 (1978) 743–768.

Chandrasekhar, S., *Hydrodynamic and Hydromagnetic Stability*. Oxford: Clarendon Press (1961).

Clever, R.M. and Busse, F.H., Instabilities of longitudinal rolls in an inclined layer. *J. Fluid Mech.* 81 (1977) 107–127.

Clever, R.M. and Busse, F.H., Nonlinear oscillatory convection. *J. Fluid Mech.* 176 (1987) 403–417.

Clever, R.M. and Busse, F.H., Nonlinear oscillatory convection in the presence of a vertical magnetic field. *J. Fluid Mech.* 201 (1989) 507–523.

Gershuni, G.Z. and Zhukhovitskii, E.M., *Convective Stability of Incompressible Fluids*. Translated from the Russian by D. Louvish. Keter Publications, Jerusalem (1976).

Hart, J.E., The stability of flow in a differentially heated inclined box. *J. Fluid Mech.* 47 (1971) 547–576.

Nagata, M. and Busse, F.H., Three-dimensional tertiary motions in a plane shear layer. *J. Fluid Mech.* 135 (1983) 1–26.

Ruth, D.W., Hollands, K.G.T. and Raithby, G.D., On free convection experiments in inclined air layers heated from below. *J. Fluid Mech.* 96 (1980a) 461–469.

Ruth, D.W., Raithby, G.D. and Hollands, K.G.T., On the secondary instability in inclined air layers. *J. Fluid Mech.* 96 (1980b) 481–492.

Schinkel, W.M.M., *Natural convection in inclined air-filled enclosures*. Dutch Efficiency Bureau, Pijnacker (1980) 342 pp.